A New, Low-Cost, Switched Beam and Fully Adaptive Antenna Array for 2.4 GHz ISM Applications

Stelios A. Mitilineos, *Student Member, IEEE*, and Christos N. Capsalis

***Abstract*—A new, low-cost, switched-beam and fully adaptive antenna array suitable for 2.4 GHz ISM applications is proposed in this paper. The array comprises of four elements, equal in number receiving RF and IF components, as well as a microcontroller based unit which is responsible for the control of the array. The array is designed with the aid of a custom genetic algorithm, while measurements results are presented indicating consistency between design and implementation. In addition, multipath fading mitigation capability of the array is demonstrated via channel measurements results.**

***Index Terms*—Adaptive array, analog beamforming, multipath fading, switched-beam array, 2.4 GHz ISM applications.**

I. Introduction

ADAPTIVE antenna arrays, or smart antennas, have been suggested in order to satisfy the increasing demand for higher data rates and enhance system capacity and spectral efficiency, thus overcoming the lack of unlimited channel bandwidth. Smart antennas are used for space and radiation pattern diversity, space division multiple access, as well as for the development of new services such as direction of arrival estimation, position location and other [1]. Furthermore, recent information theory results have demonstrated the possibility of expanding Shannon theorem in the case where multiple input multiple output (MIMO) systems are used [2].

In the literature, practical smart antenna systems are presented. Alonso *et al.* proposed a phased array for mobile satellite communications [3]. Jeon *et al.* fabricated a hybrid smart antenna system operating at 5.8 GHz [4]. Denidni *et al.* proposed a dual-antenna array incorporating one degree of freedom [5], which implements a custom algorithm [6]. Song *et al.* implemented a planar phased array for WLAN applications [7].

A new, adaptive, receiving antenna array is presented in this paper, designed to operate at the 2.4 GHz ISM band. The array is uniform circular and consists of four elements, equal in number receiving RF and IF circuits, and a microcontroller (uC) based control-unit. Current coefficients are optimized with the aid of a custom genetic algorithm (GA), while receiving circuits are designed using ADS by Agilent. Measurements results are presented and consistency between design and implementation is demonstrated. Due to the control-unit, the proposed array is fully programmable and able to drive arbitrary, user-defined switched-beam or fully adaptive algorithms. In addition, channel measurements results in a heavy clutter indoor environment are conducted, in order to demonstrate the multipath fading mitigation capability of the proposed array, in either switched-beam or adaptive mode.

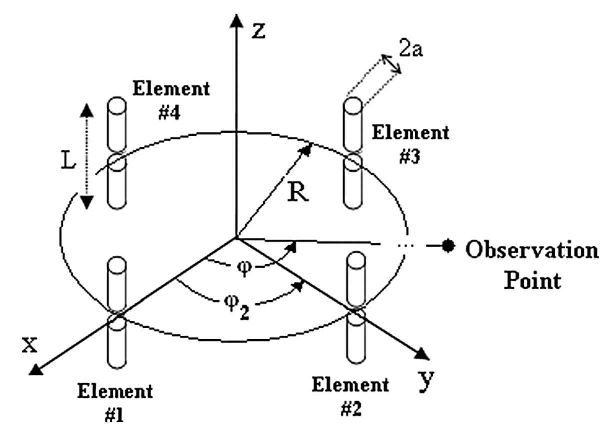

Fig. 1. Layout of the proposed array.

The rest of the paper is organized as follows: in Section II, the implemented array's architecture and functionality is illustrated. In Section III, the electromagnetic design of the array is analyzed. The design of the array RF-IF front-end is performed using ADS, and the respective components are presented in Section IV. Measurements results, demonstrating the suitability of the design and agreement to implemented array are illustrated in Section V, while channel measurements results are presented in Section VI. The paper concludes with Section VII.

II. Architecture and Functionality of the Proposed Array

The proposed array consists of four elements, placed parallel to the z-axis and uniformly arranged in a circle of radius R, as shown in Fig. 1. The elements are of type IN2458-5RD, by ConnexWireless, with a uniform gain of 2.2 dBi at the 2.4–2.5 GHz band [8].

The architecture of the receiving circuits is illustrated in Fig. 2. In the RF stage, the received signal is first filtered, then amplified by a low noise amplifier (LNA) and finally down-converted and fed to the IF stage via a mixer.

Manuscript received January 27, 2006; revised March 5, 2007.

The authors are with the Division of Information Transmission Systems and Material Technology, School of Electrical and Computer Engineering, National Technical University of Athens (NTUA), Athens 157 73, Greece (e-mail: smitil@mail.ntua.gr; ccaps@central.ntua.gr).

Digital Object Identifier 10.1109/TAP.2007.904067

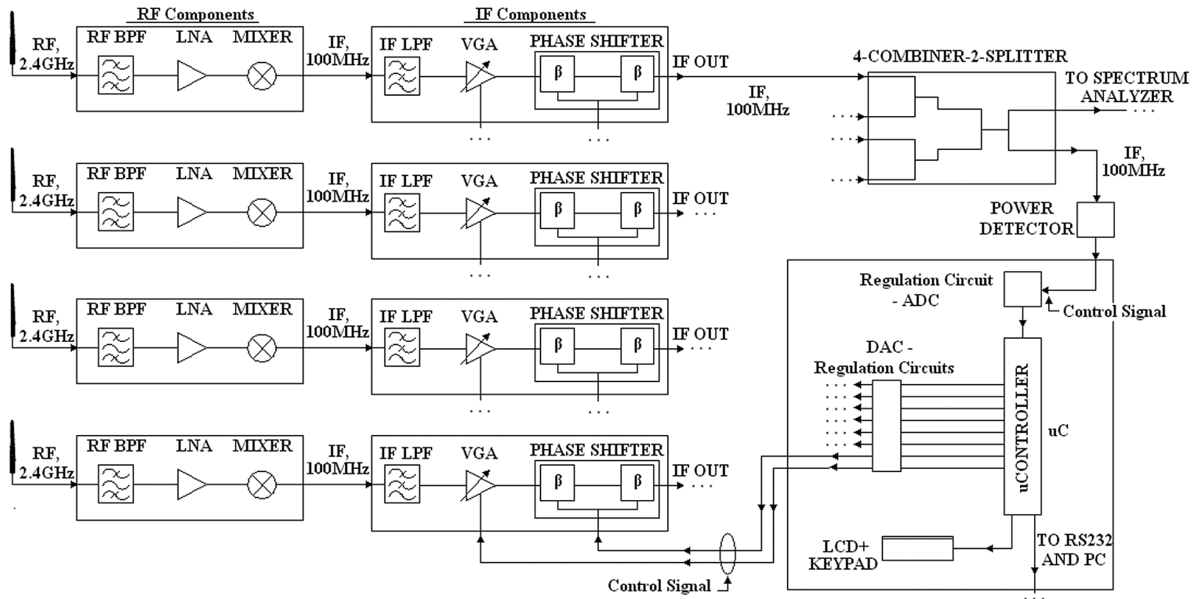

Fig. 2. Architecture of the receiving circuits.

The IF stage consists of a lowpass filter, a variable gain amplifier (VGA) and a voltage controlled phase shifter (VCPS). The VGA appropriately amplifies the received signal, according to the voltage applied to its control pin. Similarly, the VCPS shifts the signal's phase according to its control voltage input. Thus, the voltage output of each IF stage is fully controlled in amplitude and phase.

All IF outputs are vector summed by a 4-combiner-2-splitter component. The 4-combiner-2-splitter's output signals are identical to one another and are fed to a spectrum analyzer and a power detector, for measuring and control purposes, respectively. The power detector provides a baseband signal whose amplitude is proportional to the power of its input.

Power detector's output is regulated, digitally converted via an analog-to-digital converter (ADC), and then fed to the uC. Considering that maximization of the power detector's output signal amplitude is required, the uC appropriately feeds an 8-port digital-to-analog converter (DAC), whose outputs are regulated and fed to the control pins of the VGAs and VCPSs, thus establishing a closed-loop control architecture. By appropriately selecting the voltages imposed to the control pins of the VGAs and the VCPSs, any desired switched-beam or adaptive beamforming algorithm can be implemented.

The uC is also connected to a personal computer (PC) via an RS232 port, which allows for sophisticated monitoring capabilities or for complicated and memory demanding control algorithms to be performed.

III. Design of the Array

For modeling purposes, the array is assumed to consist of identical linear elements, placed vertically to the $x-y$ plane, while the center of the array corresponds to the origin of the coordinates system, as illustrated in Fig. 1. The first element is always placed at $(R, 0)$ without loss of generality. The frequency of operation is specified at 2.4 GHz, in which the wavelength is $\lambda = 0.125$ m.

TABLE I
EXCITATION COEFFICIENTS OF THE ARRAY

	Element #	Current Coefficients	Voltage Coefficients (Measured Impedance Matrix)
Relative Magnitude (Volt)	1	1.00	1.00
	2	1.13	1.13
	3	1.08	1.18
	4	0.98	1.32
Relative Phase (radians)	1	0.00	0.00
	2	0.12	0.33
	3	-1.93	-2.03
	4	-1.77	-1.52
Circle Radius (m)		**0.0625**	**0.0625**

For switched beam operation, the array shall cover the horizontal plane with four, switching and symmetrical radiation patterns, pointing towards 45°, 135°, 225°, and 315°. The beamwidth of the main beam lobes at the horizontal plane is 45°, while maximum relative side lobe level (R.S.L.L.), defined as ratio of main to maximum side lobe amplitude, is intended.

Since only the $x-y$ plane is of interest, the radiation pattern of the array, $U(\phi)$, is given by

$$U(\phi) = U_0 \left|AF(\phi)\right|^2 \tag{1}$$

where U_0 represents the pattern of each element, $AF(\phi)$ represents the array factor and ϕ is the angle of observation in the $x-y$ plane.

Since the array is uniform circular, the array factor is given by [9]

$$AF(\phi) = \sum_{m=1}^{4} c_m \exp\left(\mathrm{j}kR\cos(\phi - \phi_m)\right) \tag{2}$$

where $c_m = I_m/I_1$ are the relative current excitation coefficients, I_1 being the excitation of reference the first element (note

TABLE II
IMPEDANCE MATRIX OF THE IMPLEMENTED ARRAY

Element #	1	2	3	4
1	47.5000 + 0.5000i	2.7000 - 0.0800i	-1.0000 + 0.7500i	2.9000 - 0.6200i
2	2.7000 - 0.0800i	48.7000 +10.5000i	2.8500 + 0.0100i	-1.8000 - 0.7400i
3	-1.0000 + 0.7500i	2.8500 + 0.0100i	54.5000 - 8.7000i	2.0000 + 0.1300i
4	2.9000 - 0.6200i	-1.8000 - 0.7400i	2.0000 + 0.1300i	62.1000 +16.8000i

that c_m may be a complex number). Furthermore, $k = 2\pi/\lambda$, while R is the circle radius, and ϕ_m is the angular position of the mth element.

In addition, the excitation currents vector, $\boldsymbol{I}$, is related to the excitation voltages vector, $\boldsymbol{V}$, by the impedance matrix $\boldsymbol{Z}$ using

$$\boldsymbol{V} = \boldsymbol{Z} \cdot \boldsymbol{I}. \tag{3}$$

The impedance matrix is used in order to model mutual coupling among elements. As already pointed out, the array design is for switched-beam as well as adaptive operation. However, in the case of adaptive operation, the excitation coefficients evolve in time based to a given algorithm. At the same time, pattern calculation is easier if there exists weaker rather than stronger coupling (as R decreases, coupling increases, and vice versa). Furthermore, spatial correlation decreases as element spacing increases [2], [10], [11]. On the other hand, large values of R result to large distances among array elements, therefore the main lobe beamwidth decreases and grating lobes appear (similarly to uniform linear array theory [9] and relative results on switched parasitic arrays [12]). As a result, a circle radius of $R = \lambda/2$ is selected as a compromise between increased beamforming capability, for switched-beam operation, and poor coupling or spatial correlation among elements, for adaptive or MIMO operation, respectively.

As long as excitation optimization is concerned, a tool for antenna array design has been developed in MATLAB [13] based on the GA toolbox by Houck *et al.* [14]. GAs are a stochastic class of optimization algorithms, whose robustness has made them extremely popular among researchers. They have been introduced in the early 1960s, but only recently have they been proposed for electromagnetic optimization, and they are used all the more lately in a variety of applications, including antenna design and optimization [15]–[18]. Our tool is used herein in order to derive an optimum solution in terms of applicability.

The optimized current excitation coefficients for a four-element switched-beam array are tabulated in Table I. In order to evaluate coupling among the array elements actually used (IN2458-5RD-S by ConnexWireless), the impedance matrix of the array is measured and tabulated in Table II. Evidently, mutual coupling is found to be significantly low (6.25%, defined as ratio of mutual-impedance magnitude to self-impedance magnitude, worst case). Then, the array voltage coefficients are calculated using (3), and included in Table I. Note that the IF stages' voltage outputs are properly calibrated, in order that the relative excitations of the array elements correspond to the optimized values of Table I.

IV. ELECTRONIC COMPONENTS OF THE RECEIVER

All electronic components are custom designed using low cost off-the-shelf ICs and lumped elements, as well as easily repeatable PCB circuits. The ADS suite by Agilent was used during design and simulation. The well-known FR4 substrate, with $\varepsilon_r = 4.6$, $\tan D = 0.013$ and thickness $H = 1.5$ mm was utilized for the fabrication of microstrip circuits. The RF and IF circuits are designed as dual-layer PCBs with plated vias and SMT components, while the uC based control unit is designed as single-layer PCB in which pin-elements are used. All components are manufactured within the Antenna Laboratory in the School of the Electrical and Computer Engineering at the National Technical University of Athens (NTUA).

A block diagram of the RF stage is included in Fig. 2. The RF stage consists of an RF bandpass filter, an LNA and a down-conversion mixer. The measured attenuation of the filter is 0.4 dB; the 3-dB bandwidth is 670 MHz and the 10-dB cutoff frequencies are 1810 and 2980 MHz. The reflection coefficients are well below -18 dB within the 2.4–2.5 GH ISM band. On the other hand, MGA86576 by Agilent was used for the LNA implementation [19]. LNA's gain and noise figure are 25 and 2.4 dB, respectively, whereas input and output reflection coefficients are below -16 dB at the 2.4–2.5 GHz band. The IAM91563 by Agilent was used for the mixer implementation [20]. The mixer down-converts the signal from 2.4 GHz to 100 MHz, with a conversion gain of 6 dB. The input and output reflection coefficients of the mixer are below -16 dB and -12 dB, respectively. Also, the reflection coefficient at the local oscillator (LO) input pin is below -17 db.

The RF stage is followed by the IF stage. There is a low-pass IF filter, implemented using seven L-C lumped elements. Its 3-dB upper frequency is 145 MHz and the 10-dB cutoff frequency is 160 MHz. The reflection coefficients are below -10 dB while transmission attenuation is 0.4 dB. The VGA is fabricated using AD8367 by Analog Devices [21]. The gain range of the VGA is [-2.2 dB, 28.5 dB] for a control voltage range of [0 Volt, 1 Volt], respectively. The reflection coefficients of the VGA are always below -15 dB at 100–200 MHz, for all control voltages. The VCPS is manufactured using two cascaded JSPHS-150 passive phase shifters by MiniCircuits [22] with short-circuited control pins. The 3 dB operation band of the VCPS is 85–205 MHz, and the input and output coefficients are below -18 dB. The phase shift range is greater than 400° for a control voltage range within [0 Volt, 8 Volt], at the 100–150 MHz band.

The 4-Combiner-2-Splitter is a lumped-elements circuit, based on the well-known Wilkinson combiner component. Its reflection coefficients are below -12 dB and the attenuation from an input to an output port is 9.8 dB.

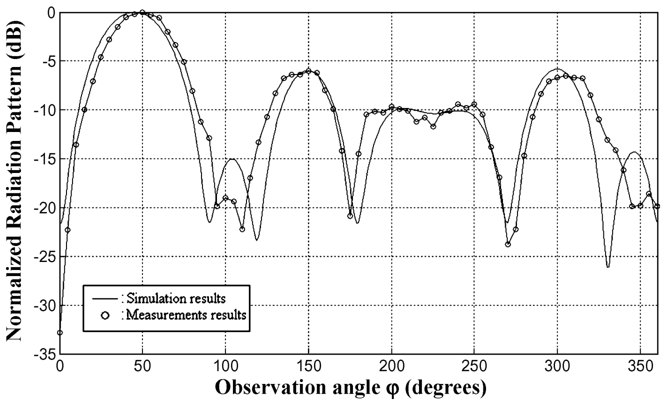

Fig. 3. Simulated and measured radiation pattern, main lobe at 45°.

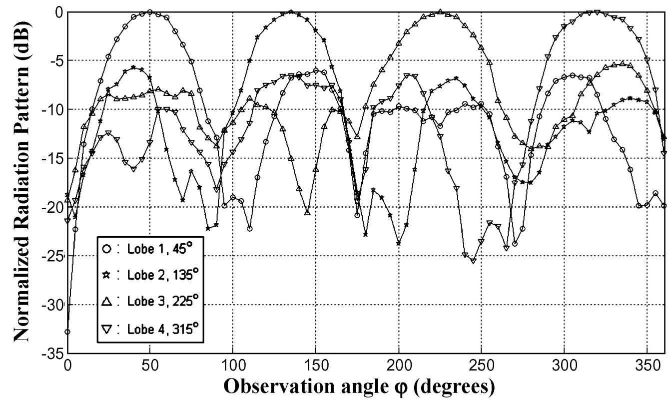

Fig. 4. Measured radiation patterns, main lobes at 45°, 135°, 225° and 315°.

The power detector is a two-input component based on AD8302 by Analog Devices [23]. Its input coefficients are kept below −16 dB. A local generated reference signal, with frequency and power equal to 100 MHz and −30 dBm, respectively, is fed to the one input of the detector. A baseband output signal indicates the relative power between the two inputs.

A uC based unit is responsible for the control of the array. It includes an ADC (type MAX118 by Maxim [24]) for reading the output of the power detector, the uC (type ATmega8535, RISC architecture microcontroller by Atmel [25]), and a DAC (type MX7228 by Maxim [26]) which feeds the control pins of the IF circuits of the array. There are also interconnections from the uC to an LCD display, a custom keypad and a PC (via RS232, using MAX232 by Maxim [27]). The ADC and DAC are preceded and followed respectively by properly adjusted operational amplifiers (OpAmps), for isolation and regulation purposes. The OpAmps are of type MXL1014 by Maxim [28].

V. Numerical and Measurements Results

The simulated radiation pattern pointing towards 45°, which is calculated using the current coefficients of Table I, is displayed in Fig. 3. The remaining three simulated radiation patterns are not displayed, since they arise after proper permutation of the excitation coefficients due to symmetry.

The array's radiation patterns are measured in the anechoic chamber of NTUA. A Hewlett-Packard 8714C network analyzer was used for the generation of a 2.4 GHz scarrier with 10 dBm output power. The EM-6961 1–18 GHz horn antenna by ElectroMetrics, with 8.7 dBi gain at the specified frequency, was used as a transmitting antenna. An Avionics IFR2031 signal generator and a custom-implemented 4-splitter provided the 2.3 GHz local oscillator input to the mixers. An Agilent E4403B spectrum analyzer was used for measuring the received power by the array. The turntable of the DAMS-5000 antenna measurement system by Diamond was used in order to accurately rotate the array. The calibration of the IF gains and phase shifts was implemented with the aid of a Hewlett-Packard 54645D mixed-signal oscilloscope.

The array's normalized radiation patterns are illustrated in Fig. 4. A comparison between measured and simulated radiation patterns is provided by Fig. 3, in the case of the 45° main beam radiation pattern. From Fig. 3, it is deducted that the measured pattern fits very well to the simulated one, while similar conclusions are valid for the rest radiation patterns.

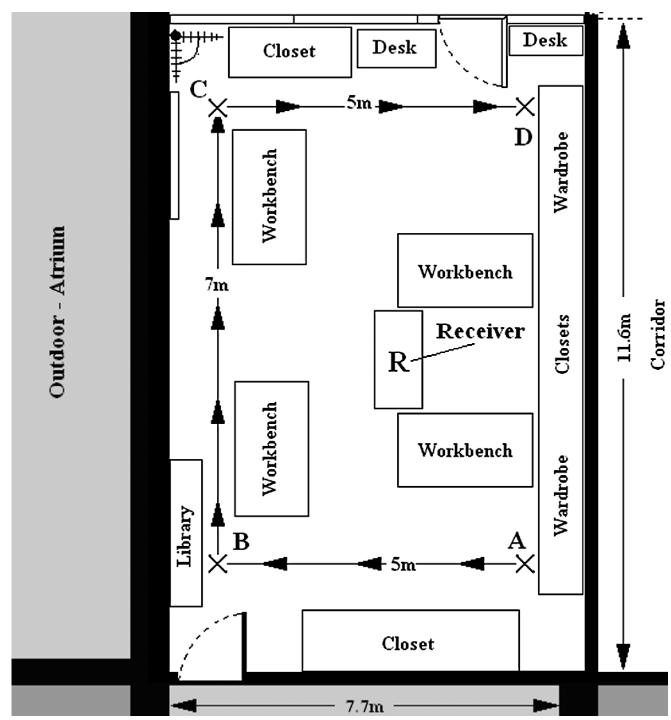

Fig. 5. A strong multipath indoor environment.

VI. Performance of the Array

A set of received signal strength (RSS) measurements has been collected within the main room of the Antenna Laboratory at NTUA, in order to demonstrate the usefulness of the proposed array. The specific radio channel is displayed in Fig. 5, and is characterized by heavy clutter due to furniture and measurements equipment (closets, workbenches, desks, as well as antennas, measurements instruments, large reflectors, etc.). The transmitter is an omnidirectional antenna of the type IN2458-5RD by ConnexWireless, and is moving with a constant low speed of 1 m/sec along the predetermined path denoted by AB-BC-CD in Fig. 5. The receiver is either an identical omnidirectional antenna or the proposed array, and is

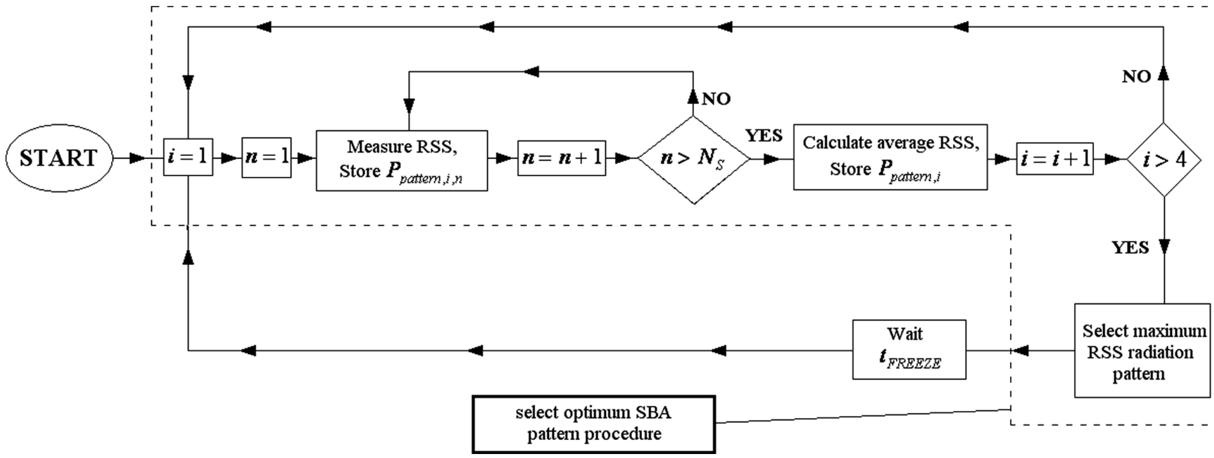

Fig. 6. Flow chart of the switched-beam algorithm.

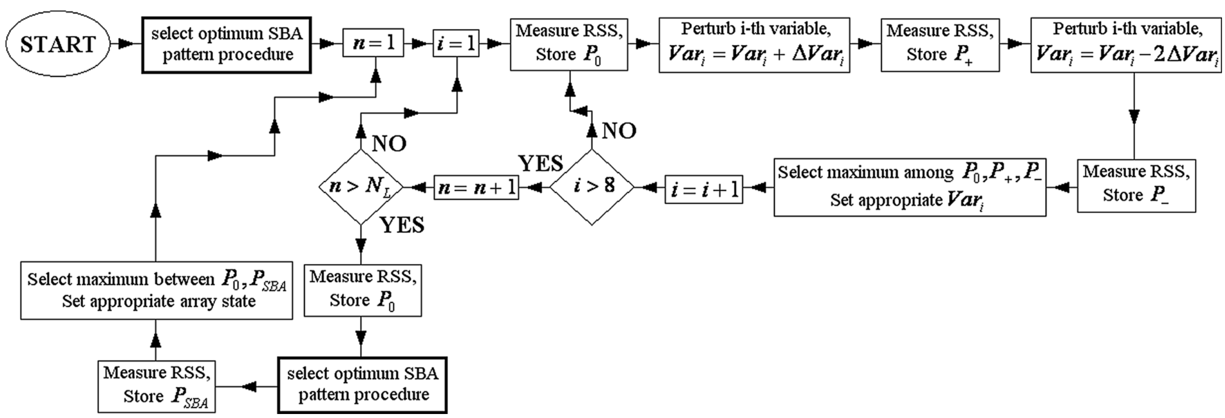

Fig. 7. Flow chart of the proposed adaptive algorithm.

kept fixed at the center of the room. Non-line-of-sight (NLOS) propagation conditions are preserved by adjusting a large metallic surface between transmitter and receiver positions.

The proposed array is operating in either switched-beam or adaptive mode. The flow chart of the switched-beam algorithm used in the former case is illustrated in Fig. 6. Essentially, the switched-beam algorithm consists in selecting the radiation pattern which corresponds to the maximum RSS. This is accomplished by sampling each pattern's RSS with a desired number of samples, N_S, then calculating the average signal strength, and finally selecting the optimum pattern. The array state is locked for a predetermined time interval, t_{FREEZE}, and then the procedure is repeated infinitely.

The dashed line in Fig. 6 indicates the "select optimum SBA pattern" procedure, and is used by the adaptive algorithm proposed herein. Thus, the adaptive algorithm initially estimates and locks at the maximum RSS radiation pattern, as illustrated in Fig. 7. Then, the algorithm enters a double loop, where the array VGAs' and VCPSs' control voltages are sequentially perturbed, searching for larger RSS values. The VGAs' and VCPSs' control voltage values are bounded within [0 Volt, 1 Volt] and [0 Volt, 8 Volt], respectively. After a predetermined number of loop executions, N_L, the adaptive algorithm compares the achieved signal strength to that delivered by the predetermined SBA radiation patterns, in order to mitigate

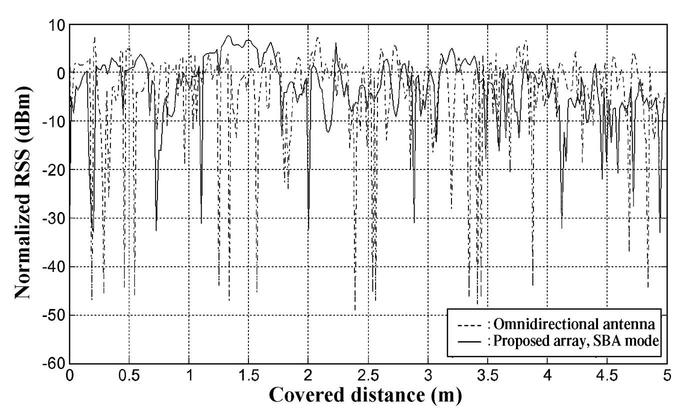

Fig. 8. RSS measurements snapshot, omnidirectional antenna and proposed array in SBA mode.

possible deadlocks in local optima. In any case, the array state which corresponds to the maximum received signal strength is selected (adaptively-reached state or SBA-predetermined state), and the procedure is repeated infinitely.

A large set of RSS measurements is collected, using either the omnidirectional receiver or the proposed array. Fig. 8 displays a snapshot of the recorded RSS in the case where either the omnidirectional receiver or the switched-beam algorithm is used, while a respective snapshot is displayed in Fig. 9 in the

TABLE III
PERFORMANCE OF THE PROPOSED ARRAY

		Omnidirectional Receiver	SBA	Adaptive Receiver
Mean RSS		-44.34dBm	-21.56dBm	-20.11dBm
Maximum Fade Depth		56.18dB	40.12dB	39.45dB
Fade Level Crossings	10dB	39	20	16
	20dB	22	10	5
	30dB	16	7	2
	40dB	15	0	0
	50dB	0	0	0
Average Fade Duration	10dB	15.2%	11.2%	11.1%
	20dB	6.3%	4.5%	2.1%
	30dB	4.6%	3.3%	0.8%
	40dB	4.3%	0.0%	0.0%
	50dB	0.0%	0.0%	0.0%

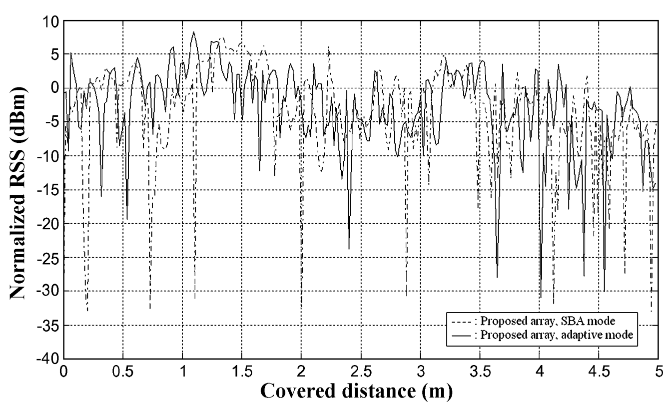

Fig. 9. RSS measurements snapshot, proposed array in SBA and adaptive mode.

case where the switched-beam or the adaptive algorithm is used. Both snapshots correspond to the path AB of Fig. 5. The evaluation of the array for the snapshots of Fig. 8 and Fig. 9 is based on the maximum fade depth, fade level crossings and average duration of fades [10], and is summarized in Table III. Evidently, all channel statistics are significantly improved as we move on from the omnidirectional receiver to the SBA and from the SBA to the adaptive array. Similar results have been observed for the entire RSS measurements set.

VII. CONCLUSION

A fully adaptive and switched beam array has been designed and implemented using inexpensive commercial components. Measurements results show consistency between array design and implementation. The array is fully programmable and may be used with user-defined switched-beam or adaptive algorithms. Using the measured impedance matrix, and based on the fact that mutual coupling is low, it is expected that the radiation pattern of the array will be calculated with sufficient accuracy for any IF gain or phase shift may arise due to an arbitrary adaptive algorithm. The usefulness of the array is demonstrated via RSS measurements in a strong multipath indoor environment, where multipath fading is mitigated to a large extent.

ACKNOWLEDGMENT

The authors would like to thank K. Mougiakos for his help during the design and implementation of the control unit of the array, as well as Prof. G. Fikioris for his help during the revision of the paper. S. A. Mitilineos would also like to thank Dr. G. Mitropoulos for his stirring support during the preparation and revision of the paper, as well as Dr. Y. Stratakos for helpful discussions.

REFERENCES

[1] J. C. Liberti and T. S. Rappaport, *Smart Antennas for Wireless Communications: IS-95 and Third Generation CDMA Application*. Upper Saddle River, NJ: Prentice-Hall, 1999.
[2] A. Paulraj, R. Nabar, and D. Gore, *Introduction to Space-Time Wireless Communications*. Cambridge, U.K.: Cambridge Univ. Press, 2003.
[3] J. I. Alonso, J. M. Blas, L. E. Garcia, J. Ramos, J. de Pablos, J. Grajal, G. G. Gentili, J. Gismero, and F. Perez, "Low cost electronically steered antenna and receiver system for mobile satellite communications," *IEEE Trans. Microw. Theory Tech.*, vol. 44, no. 12, pp. 2438–2449, Dece. 1996.
[4] S. S. Jeon, Y. Wang, Y. Qian, and T. Itoh, "A novel smart antenna system implementation for broadband wireless communications," *IEEE Trans. Antennas Propag.*, vol. 50, no. 5, pp. 600–606, May 2002.

[5] T. A. Denidni, D. McNeil, and G. Y. Delisle, "Experimental investigations of a new adaptive dual-antenna array for handset applications," *IEEE Trans. Veh. Technol.*, vol. 52, no. 6, pp. 1417–1423, Nov. 2003.

[6] T. A. Denidni and G. Delisle, "A nonlinear algorithm for output power maximization of an indoor adaptive phased array," *IEEE Trans. Electromagn. Compat.*, vol. 37, pp. 201–209, May 1995.

[7] C. T. P. Song, A. Mak, B. Wong, D. George, and R. D. Murch, "Compact low cost dual polarized adaptive planar phased array for WLAN," *IEEE Trans. Antennas Propag.*, vol. 53, no. 8, pp. 2406–2416, Aug. 2005.

[8] IN2458-5RD Specifications Datasheet, Rev. 2 Mar. 21, 2005, ConnexWireless.

[9] C. A. Balanis, *Antenna Theory: Analysis and Design*. New York: Wiley, 1997.

[10] G. L. Stuber, *Principles of Mobile Communication*. Norwell, MA: Kluwer Academic, 2001.

[11] J. Luo, J. R. Zeidler, and S. McLaughlin, "Performance analysis of compact antenna arrays with MRC in correlated Nakagami fading channels," *IEEE Trans. Veh. Technol.*, vol. 50, no. 1, pp. 267–277, Jan. 2001.

[12] C. Sun, A. Hirata, T. Ohira, and N. C. Karmakar, "Fast beamforming of electronically steerable passive array radiator antennas: Theory and experiment," *IEEE Trans. Antennas Propag.*, vol. 52, no. 7, pp. 1819–1831, Jul. 2004.

[13] S. A. Mitilineos and C. N. Capsalis, "On array failure mitigation using genetic algorithms and a priori joint optimization," *IEEE Antennas Propag. Mag.*, vol. 47, no. 4, pp. 227–232, Aug. 2005.

[14] C. R. Houck, J. A. Joines, and M. G. Kay, A genetic algorithm for function optimization: A MATLAB implementation NCSU-IE TR 95-09, 1995.

[15] R. L. Haupt, "An introduction to genetic algorithms for electromagnetics," *IEEE Antennas Propag. Mag.*, vol. 37, no. 2, pp. 7–15, Apr. 1995.

[16] E. A. Altshuler and D. S. Linden, "Wire-antenna designs using genetic algorithms," *IEEE Antennas Propag. Mag.*, vol. 39, no. 2, pp. 33–43, Apr. 1997.

[17] J. M. Johnson and Y. R. Samii, "Genetic algorithms in engineering electromagnetics," *IEEE Antennas Propag. Mag.*, vol. 39, no. 4, pp. 7–21, Aug. 1997.

[18] Y. R. Samii and E. Michielssen, *Electromagnetic Optimization by Genetic Algorithms*. New York: Wiley, 1999.

[19] MGA86576 1.5–8 GHz Low Noise GaAs MMIC Amplifier, Technical Data HP.

[20] IAM91563 0.8–6.0 GHz 3 V Downconverter, Technical Data Agilent Technologies.

[21] AD8367 500 MHz, Linear-in-dB VGA With AGC Detector Datasheet Analog Devices.

[22] Phase Shifters, Plug-in and Surface Mount, 180 ° Voltage Variable Datasheet MiniCircuits.

[23] AD8302 LF-2.7 GHz RF/IF Gain and Phase Detector Datasheet Analog Devices.

[24] MAX114/MAX118 +5 V, 1 Msps, 4&8 Channel, 8-bit ADCs Datasheet Maxim.

[25] ATmega8535/ATmega8535L 8-bit AVR 8 KBytes Flash Microcontroller Datasheet Atmel.

[26] MX7228 CMOS Octal 8-bit D/A Converter Datasheet Maxim.

[27] MAX220–MAX249 +5 V, Multichannel RS232 Drivers/Receivers Datasheet Maxim.

[28] MXL1013/MXL1014 Dual/Quad Precision OpAmps Datasheet Maxim.

Stelios A. Mitilineos (S'01) was born in Athens, Greece, in 1977. He received the Diploma in Electrical and Computer Engineering from the National Technical University of Athens (NTUA), in October 2001, where he is currently working toward the Ph.D. degree.

His research interests are in the areas of antennas and propagation, smart antennas and mobile communications, microwave components and MIMO systems, and position location.

Christos N. Capsalis was born in Nafplion, Greece, in 1956. He received the Diploma in Electrical and Mechanical Engineering and the Ph.D. degree in electrical engineering from the National Technical University of Athens (NTUA), Athens, Greece in 1979 and 1985, respectively, and the Diploma in Economics from the University of Athens, in 1983.

He is currently a Professor with the Electrical and Computer Engineering Department at NTUA. His current scientific activity concerns satellite and mobile communications, antenna theory and design, and electromagnetic compatibility.